UVicSPACE: Research & Learning Repository

University of Victoria

Faculty of Science

Faculty Publications

Probing the Microenvironments in a Polymer-Wrapped Core−Shell Nanoassembly Using Pyrene Chromophores

Tuoqi Wu, Jessy Oake, Zhongde Liu, Cornelia Bohne, and Neil R. Branda

July 2018

This is an open access article published under an ACS AuthorChoice License, which permits copying and redistribution of the article or any adaptations for non-commercial purposes.

This article was originally published at:

http://dx.doi.org/10.1021/acsomega.8b00953

Wu, T., Oake, J., Liu, Z., Bohne, C. & Branda, N.R. (2018). Probing the Microenvironments in a Polymer-Wrapped Core-Shell Nanoassemble Using Pyrene Chromophores. *ACS Omega*, *3*(7), 7673-7680. http://dx.doi.org/10.1021/acsomega.8b00953

This is an open access article published under an ACS AuthorChoice License, which permits copying and redistribution of the article or any adaptations for non-commercial purposes.

ACS OMEGA

Article

Cite This: ACS Omega 2018, 3, 7673−7680

Probing the Microenvironments in a Polymer-Wrapped Core−Shell Nanoassembly Using Pyrene Chromophores

Tuoqi Wu,[†,§] Jessy Oake,[‡,§] Zhongde Liu,[†,∥] Cornelia Bohne,*[,‡] and Neil R. Branda*[,†]

[†]4D LABS, Department of Chemistry, Simon Fraser University, 8888 University Drive, Burnaby, British Columbia V5A 1S6, Canada

[‡]Department of Chemistry and Centre for Advanced Materials and Related Technologies (CAMTEC), University of Victoria, P.O. Box 1700 STN CSC, Victoria, British Columbia V8W 2Y2, Canada

Supporting Information

ABSTRACT: The local environments within an amphiphilic polymer shell wrapped around lanthanide-doped upconverting nanoparticles were probed using steady-state and time-resolved fluorescence spectroscopy techniques. Emission lifetime measurements of pyrene chromophores trapped within the polymer shell reveal that there are at least two environments, where the organic pyrene molecules are encapsulated in hydrophobic environments that have lower polarity than in water. The migration of pyrene chromophores from their initial location to another location was also observed, demonstrating that the polymeric shell provides both hydrophobicity and mobility for entrapped molecules. These results offer insight into what outcomes can be expected when chemical reactions are carried out in these nanoassemblies, especially if they are to be used as nanoreactors for synthesis or delivery vehicles for therapeutics.

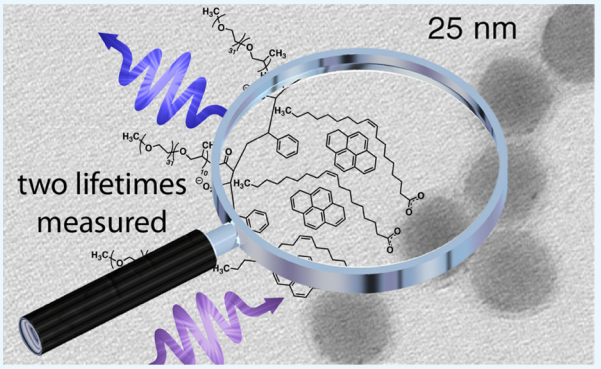

1. INTRODUCTION

Water-dispersible nanoassemblies composed of amphiphilic polymers wrapped around inorganic nanoparticles offer confined lipophilic spaces that sequester hydrophobic species from the bulk aqueous environment (Figure 1). These microenvironments can result in significant changes in how the encapsulated molecules behave compared to the same molecules dispersed in bulk solution.[1] The changes in properties of molecules within a confined microenvironment include molecular dynamics,[2] fluorescence,[3] bond vibrations,[4] binding affinities,[5] and electrochemistry.[6]

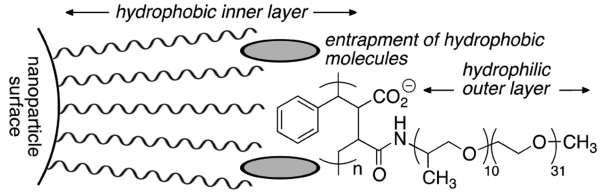

Figure 1. Proposed structure of the water-dispersible nanosystem. Amphiphilic polymers encapsulate inorganic nanoparticles and provide a hydrophobic inner layer where hydrophobic molecules can be trapped. The hydrophilic outer layer renders the entire assembly water dispersible.

Previously, we showed that the reversible photochemical reactions of hydrophobic chromophores, which typically require nonpolar organic solvents for optimal performance (the reactions are significantly suppressed in water), can be carried out to the same extent in water when they are entrapped within a nanoassembly's polymeric shell.[7−10] In these cases, the nanoparticles are upconverting nanoparticles (UCNPs) composed of crystalline $NaYF_4$ doped with trivalent lanthanide ions such as Er^{3+} and Tm^{3+}, which have the interesting optical property that they absorb multiple photons of 980 nm near-infrared light and combine them to emit UV and visible photons of several wavelengths in the electromagnetic spectrum.[11,12] We have used these UCNPs to activate reversible photochemical reactions of small photochromic molecules encapsulated in water-dispersible nanoassemblies. Clearly, the fact that the photochemical behavior observed in nonpolar solvents is retained in aqueous solutions is due to the fact that the chromophores must reside in nonpolar local environments even though the entire assembly is in water. One can speculate that the chromophores are located close to the surface of the nanoparticles as this is likely to be the least polar environment (Figure 1), although this speculation requires evidence to support it. This is the focus of the studies described herein. A better understanding of the polarity of the shell will also help determine how versatile are the nanoassemblies for carrying out specific photoreactions and for trapping small molecules. For example, if free water is

Received: May 9, 2018
Accepted: June 19, 2018
Published: July 11, 2018

Downloaded via UNIV OF VICTORIA on March 27, 2019 at 19:55:55 (UTC).
See https://pubs.acs.org/sharingguidelines for options on how to legitimately share published articles.

© 2018 American Chemical Society

DOI: 10.1021/acsomega.8b00953
ACS Omega 2018, 3, 7673−7680

present within the polymeric shell, many photoreactions will be affected because they are limited or completely shut down when water is present.[13−15] In other cases, such as the photochemical release of caged compounds using benzoin derivatives, water interferes with the photolysis pathway and generates different products than when carried out in "dry" environments.[16] The importance of the local environment to control photoreactions has also been highlighted when reactions are carried out within micelles or other supramolecular systems.[17,18] It is, therefore, important to predict if small molecules and reactants within confined spaces are localized in one environment with defined properties or if they are in several environments each having different properties, which could lead to different reactivities within the same assembly. Two illustrative and opposing examples are (1) sodium dodecyl sulfate micelles that incorporate molecules in one average environment display one type of reactivity, whereas (2) molecules within bile salt micelles can be located in unalike binding sites resulting in different behaviors.[19−21]

Our goals are to elucidate the microenvironments of our previously reported nanoassemblies in much more detail to provide guidelines for applying them as delivery systems and as catalysts for carrying out biphasic hydrophobic/hydrophilic reactions in a homogeneous dispersion. The focus is to identify whether the nanoassemblies have local areas of different polarities for trapping a hydrophobic molecule, which could infer that these sites have different contents of water. We chose to use encapsulated pyrene chromophores as they are commonly used fluorescent molecules to probe the polarity of local environments. This is achieved by comparing the ratio of the intensities of the first to third vibronic emission bands (I/III ratio) of the five distinct bands in the emission spectrum,[22,23] which is very sensitive to the polarity of the solvent surrounding the chromophore.[22,23] A larger I/III ratio indicates higher polarity such as when pyrene is in an aqueous solution, whereas a smaller value reflects the pyrene molecules residing in less polar conditions, as for example pyrene located in less polar solvents,[22,23] trapped within micelles, or encapsulated within dendrimers.[17,18,24] This solvent-dependent fluorescence has made pyrene one of the most versatile probes to characterize microenvironments.[17,25] In this report, we use pyrene to investigate the nature of the amphiphilic polymer shell using a combination of steady-state and time-resolved spectroscopy and show that there are at least two microenvironments existing in our nanosystems.

2. RESULTS AND DISCUSSION

The synthesis of the nanoassembly of interest is shown in Scheme 1 and follows the same general "plug-and-play" protocol we have previously used.[7,9] In the first step, cumene-terminated poly(styrene-*co*-maleic anhydride) (PSMA) is stirred with JEFFAMINE 2070 in chloroform to produce the amphiphilic polymer **P1**. Treating this polymer with the oleic acid-coated lanthanide-doped UCNPs (β-$NaYF_4$: 2 mol % Er^{3+}, 20 mol % Yb^{3+}) ($NaYF_4$:ErYb) and pyrene, followed by replacing $CHCl_3$ with basic water induces the self-assembly process and results in the final nanosystems (**P1-NP-pyr**) where the polymer is wrapped around the nanoparticle and the pyrene chromophores are trapped within the hydrophobic shell. Two batches were prepared by this procedure from the identical starting materials to compare the reproducibility of self-assembly. This route can also be used to prepare control nanoassemblies lacking the pyrene chromophores (denoted "**P1-NP**" in this paper) by omitting the pyrene in the self-assembly step.

Scheme 1. Synthesis of Pyrene-Containing Nanoassembly P1-NP-pyr

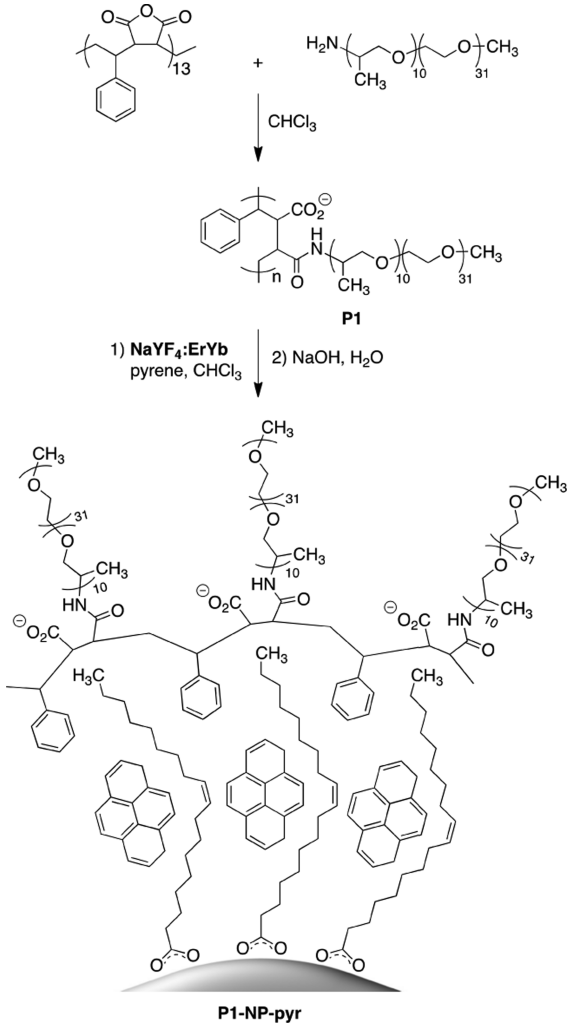

Transmission electron microscopy (TEM) images of the uranyl acetate-stained nanoassemblies show the presence of the organic shell as indicated by faint rings surrounding the darker inorganic nanoparticles for both batches of **P1-NP-pyr** (Figure 2a,b). This observation is consistent with our previously reported nanoassemblies.[7] Because the two nanoassemblies are made from the same sample of UCNPs and TEM typically shows only inorganic structures with high contrast, the average sizes of both batches are identical (average size = 24.1 ± 0.8 nm not accounting for the faint halos that surround the dark images), which correlate with that for the original oleic acid-coated UCNPs.[26] The size distribution of the nanoassemblies including the organic shells can be estimated using dynamic light scattering (DLS) techniques, which results in an average hydrodynamic diameter of 32.8 ± 0.3 nm for the first batch of **P1-NP-pyr** (Figure 2c) and 32.8 ± 0.7 for the second batch (Figure 2d).[26] If the thickness of the organic outer layer is estimated using the idealized, fully extended view of the mPEGs side chains, a value of 10−11 nm is the result. However, the combination of TEM and DLS measurements suggests thicknesses of 8.7 ± 0.9 and 8.7 ± 1.1 nm (the average size of inner UCNPs subtracted

DOI: 10.1021/acsomega.8b00953
ACS Omega 2018, 3, 7673−7680

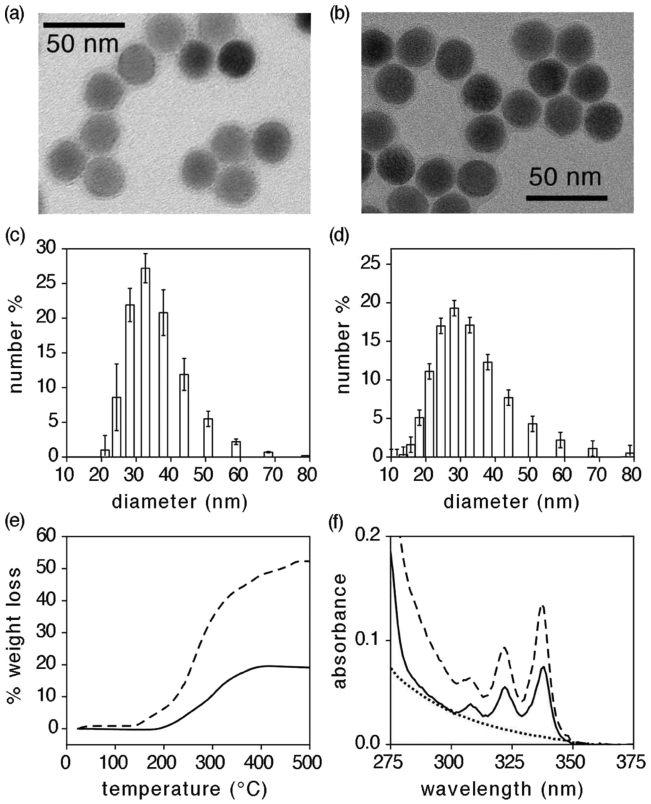

Figure 2. TEM image of uranyl acetate-stained **P1-NP-pyr** nanoassemblies (a) batch 1 and (b) batch 2 showing the UCNP core (dark inner circle) and polymeric shell (light halo). DLS measurements showing the hydrodynamic size distribution of **P1-NP-pyr** nanoassemblies dispersed in water (c) batch 1 (average size = 32.8 ± 0.3 nm) and (d) batch 2 (average size = 32.8 ± 0.7 nm).[27] (e) TGA of both batches of **P1-NP-pyr** nanoassemblies (batch 1, solid line; batch 2, dashed line). (f) UV−vis absorbance spectra of aqueous dispersions of **P1-NP-pyr** (batch 1, 1.6×10^{-6} M pyrene, solid line; batch 2, 3.4×10^{-6} M pyrene, dashed line), and the control sample without pyrene (dotted line).[28]

from the total hydrodynamic diameter), implying that in aqueous environments, the polymeric shell around the nanoparticles exists in a slightly compressed form rather than being fully extended. This result also suggests that it is unlikely that each nanoparticle is surrounded by more than one polymer layer.

The differences between the two batches are observed when the amount of organic material is analyzed using thermogravimetric analysis (TGA), which showed that there is more than twice the weight loss in the second batch than that in the first (Figure 2e). This difference in weight loss indicates that the second batch of **P1-NP-pyr** nanoassemblies must have a larger amount (2.5 times) of organic material surrounding the core UCNPs. Although these TGA measurements also show that there are more nanoparticles in batch 2 because of weighing error, this increase is less than 30% (3.04×10^{-3} g for batch 1 and 3.89×10^{-3} g for batch 2) and does not account for the 2.5 times increase in the organic material. Because DLS shows that the two batches have similar sizes, the difference in weight loss could be explained by assuming that the polymer coating is more densely packed around the nanoparticles and/or there is a higher loading of pyrene chromophores trapped within the polymer layer. The latter explanation is supported by UV−vis absorption spectroscopy, although the polymer accounts for the majority of the difference in mass. Figure 2f shows the characteristic absorption bands between 300 and 350 nm corresponding to the pyrene chromophore in an aqueous dispersion of both batches of the nanoassemblies **P1-NP-pyr**. The presence of these bands confirms the successful encapsulation of pyrene within the nanoassemblies, and the amount of chromophore measured is higher than the water solubility of pyrene (0.67×10^{-6} M).[29] Figure 2f also shows that there is substantially more pyrene (almost twice) within the polymer shell of the second batch compared to the first. On the basis of the absorbance spectra and TGA, the average number of pyrene chromophores within each batch of **P1-NP-pyr** can be estimated to be 30 for the first and 55 for the second.[26] This difference in pyrene loading may contribute to different fluorescent emission properties of the two batches as explained below.

The emission spectra (λ_{ex} = 335 nm) of aqueous dispersions of both batches of **P1-NP-pyr** are shown in Figure 3, and they

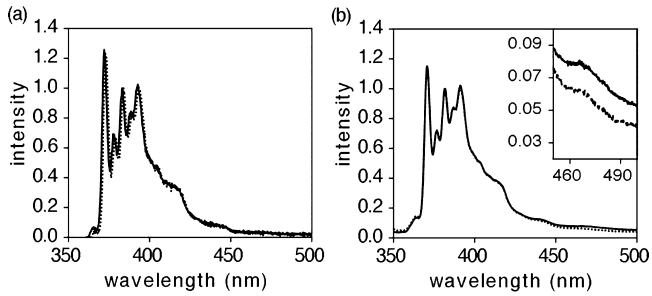

Figure 3. Normalized (to 383 nm) fluorescence spectra (λ_{ex} = 335 nm) for aqueous dispersions of (a) first batch of **P1-NP-pyr** (1.6×10^{-6} M pyrene) and (b) second batch of **P1-NP-pyr** (3.4×10^{-6} M pyrene).[28] The dotted lines are the spectra measured after a period of time (10 days for the first batch and 23 days for the second). The excimer emission in the case of the second batch, which disappears after a period of time, is shown in the inset. Any minor shifts in the peak maxima (typically 2 nm or less) between both batches can be attributed to a shift in the monochromator alignment and the determination of spectra with different bandwidths.

both show the characteristic emission from a pyrene monomer that has a progression of vibronic peaks. In the case of the first batch of the nanoassemblies, the lack of a broad emission band between 450 and 550 nm where the emission for the pyrene excimer typically appears suggests that the encapsulated chromophores are not in close proximity to each other.[17,30] This is not true for the second batch, and a weak excimer emission in the spectrum can be seen in the inset in Figure 3b. This emission is only apparent when the fluorescent spectrum is recorded shortly after the preparation of the sample, and the excimer emission disappears after a period of time (dotted line in Figure 3b). We attribute the presence of an excimer emission in the case of the second batch to the higher average number of pyrenes residing within the same volume of polymer shell as described previously. This would result in a higher probability that two or more pyrenes will be in close proximity. The fact that the excimer emission vanishes after a period of time is strong evidence, showing that the chromophores remain mobile within the polymeric shell rather than confined in one location, and they relocate into different environments over time.

Although the wavelengths at which the individual bands appear in the emission spectra of pyrene in water and

DOI: 10.1021/acsomega.8b00953
ACS Omega 2018, 3, 7673−7680

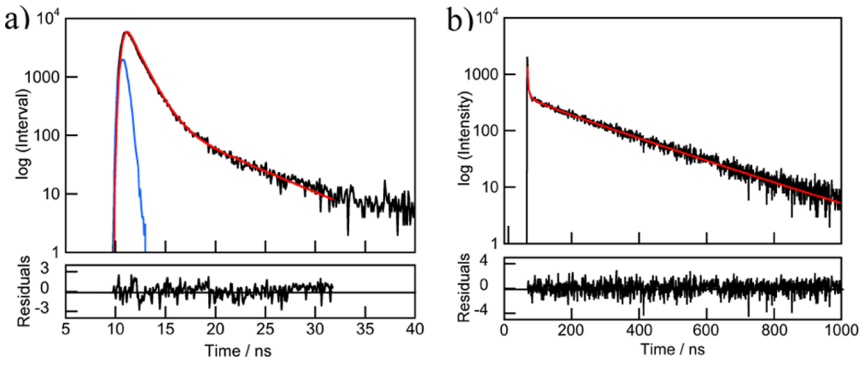

Figure 4. Fluorescence decays (black) of aqueous dispersions for (a) **P1-Np** control experiment and (b) first batch (1.6×10^{-6} M)[28] of **P1-NP-pyr** monitored at 400 nm (λ_{ex} = 335 nm). The fitting curves (red lines), instrument response function (IRF) (blue line), and residuals between the calculated and experimental data (lower panel) are also shown. No IRF is shown for the **P1-NP-pyr** emission (b) because it is narrow on this time window.

encapsulated pyrene measured with the same experimental conditions show only a small shift (Figure S3),[31] the relative intensities of bands I and III are different.[26] The I/III ratio measured for an aqueous solution of pyrene (0.5 μM) is 1.97 ± 0.01[32] but drops to 1.26 ± 0.04 for batch 1 of **P1-NP-pyr** and 1.15 ± 0.03 for batch 2. These results indicate that on average, pyrene must reside within a less polar environment than water, which presumably is the polymeric shell surrounding the UCNPs. The difference in the I/III ratios between the two batches of nanoassemblies suggests that the pyrenes are partitioned in different environments in each batch, and that there are either more pyrenes located in a less polar environment in the second batch compared to the first, or that batch 2 has more apolar environments than batch 1. At this stage, it is important to appreciate that the steady-state emission spectra in Figure 3 correspond to a weighted average of all of the pyrene chromophores residing in their different environments, where the contribution is greatest for the chromophores with the longest lifetimes. Time-resolved experiments can provide more details as to the distribution of environments as described below.

Time-resolved experiments on both batches of the nanoassembly **P1-NP-pyr** show the presence of several kinetic decay components (Figure 4).[26] Light scattering contributes to the decays as a fast component following the excitation pulse. Control experiments for **P1-NP** show an emission (Figure 4a) that in addition to the scattering can be adequately fit with two exponentials that have lifetimes shorter than 6 ns (Tables S1 and S2). Given the fact that UCNPs only absorb around 975 nm,[33] we attribute these two components to the fluorescence decay of impurities trapped within the oleic acid ligand shell. The lifetimes for the emission of the control are significantly shorter than that for pyrene and are accounted for by fixing the values in the decay for **P1-NP-pyr** and by assuming that scattering follows the instrument response function (IRF) of the system.[26] In the analysis below, we focus only on the decay of the pyrene emission. The fluorescence decays for both batches of the nanoassemblies have two long-lived components (Figure 4b) with lifetimes assigned to the pyrene emission that change upon storing the samples. When first measured, the lifetimes for batch 1 are 60 ± 20 and 217 ± 6 ns with pre-exponential factors of (14 ± 7) and (86 ± 8)% for the short and long lifetimes, respectively. For batch 2, the initial lifetimes were 29 ± 6 and 184 ± 3 ns with (30 ± 2) and (70 ± 2)% pre-exponential factors, respectively. After 3 weeks of storage, the measured lifetimes for batch 1 change to 89 ± 4 and 236 ± 1 ns, with the increased contribution of the shorter lifetime component (25 ± 2)% [compared to (14 ± 7)% initially]. For batch 2, the changes in lifetimes are smaller (34 ± 6 and 200 ± 4 ns after 3 weeks and 23 ± 4 and 213 ± 7 ns after 10 weeks) and the change in pre-exponential factors takes longer to occur [(34 ± 2) and (66 ± 2)% after 3 weeks and (55 ± 3) and (45 ± 3)% after 10 weeks] for the short and long lifetimes, respectively (Tables S1 and S2). This result emphasizes the need to perform time-resolved experiments in conjunction with steady-state ones as the I/III ratio is a composite value reflecting a weighted average when pyrenes are located in more than one environment.

Although the actual lifetimes from both batches of **P1-NP-pyr** are different, the fact that two pyrene fluorescence lifetimes are recovered from the fit of the decays in both cases indicates that the pyrene chromophores are located in at least two different environments with different properties. We are not able to differentiate between environments where excited pyrene has similar lifetimes. The presence of more than two environments, but with similar properties, is supported by the change in the absolute values of the lifetimes over time. Therefore, the analysis of the lifetime data is made at a qualitative level where two different binding regions exist, one with short lifetimes (20−90 ns) and a second one where excited pyrene has longer lifetimes (180−240 ns) than that in water (130 ns).

We do not believe that the lifetimes measured correspond to pyrene leaking out of the nanoassemblies as supported by the fact that when an aqueous dispersion of **P1-NP-pyr** is centrifuged, no emission can be detected from the supernatant, showing that it is unlikely that any of the two lifetimes recovered from the emission decay is due to "free" pyrene. Therefore, the two lifetimes observed correspond to pyrene in different environments within **P-NP-pyr**. The different lifetimes and pre-exponential factors obtained for two different batches are likely related to the different loadings of pyrene of the nanoparticles. Although a concentration dependence study of pyrene loading of the nanoparticles is beyond the objective of this study, the variability of the photophysical parameters for the pyrene emission shows that different distributions of small molecule loading of the nanosystem occur, which are not apparent from usual characterization of the system with TEM and DLS.

DOI: 10.1021/acsomega.8b00953
ACS Omega 2018, 3, 7673−7680

The lifetime for pyrene in aerated water is reported to be 130 ns.[34,35] In our measurements, the calculated lifetimes are longer, indicating that some pyrenes are located in a less polar environment than water, which is presumably within the organic polymeric shell, and this assumption is in agreement with the lower I/III ratios determined from our steady-state fluorescent measurements. The shorter lifetimes (60 ± 20 and 29 ± 6 ns) may be attributed to the fact that some pyrenes are in close proximity to the UCNP surface, resulting in energy-transfer processes that could partially quench the pyrene emission.[36,37] These results support the proposed cartoon structure of the nanoassembly shown in Figure 1. The less polar environment where pyrenes are encapsulated is provided by the hydrophobic chains of the amphiphilic polymer, and the oleic acid ligands coating UCNPs, leading to both shorter and longer lifetime components. The hydrophilic mPEG outer layer renders the nanosystem water-dispersible, and the amphiphilic polymeric shell projects water out to maintain a hydrophobic environment inside the shell for photochemistries to happen. It should be noted that the I/III ratio is not sufficiently low to eliminate the possibility that some pyrenes could be located in this outer layer, which is more polar than the inner layers.

The increased contributions of the shorter lifetimes (60 ± 20 and 29 ± 6 ns) after storage suggest that the pyrenes are gradually migrating within the polymeric shell to locations closer to the nanoparticle surface, where the pyrene fluorescence is partially quenched. This behavior also explains why the excimer emission can be observed in batch 2 of the nanoassembly initially but eventually disappears after stored at ambient condition for several days. This molecular migration phenomenon makes our nanosystem a very interesting candidate for nanoreactors because one can imagine that performing photochemistry in these nanoreactors (of which partition molecules from bulk environment but still allow partial molecular freedom) will be different compared to performing photochemistry in free solution and in strictly confined solid crystalline structures.

3. CONCLUSIONS

In summary, we have demonstrated that the emissive characteristics of pyrene chromophores are useful to probe the nature of the local environments within the amphiphilic layer of the polymer-encapsulated UCNP nanosystem. Steady-state and time-resolved fluorescence spectroscopy suggest the presence of different local environments in the polymeric shell, which are less polar than water and where the organic pyrene chromophores can reside. This explains why we[7,9] and others[38] have previously demonstrated that photoresponsive molecules retain their phototactivity in similar nanoassemblies even though the entire system is in water. We also observe the migration of the pyrene chromophores within the polymeric shell, and this property of the polymeric shell makes the nanoassembly a very interesting candidate for nanoreactors because the mobility of reagents can be exploited to control bimolecular reactivity. The work presented here should help in guiding the design of future generation nanoreactors and drug delivery vehicles, which have the potential to convert water-insoluble reagents or prodrugs into water-soluble products and drugs using UCNPs and photochemistry.

4. EXPERIMENTAL SECTION

4.1. Materials and Methods. *4.1.1. General.* Pyrene was purchased from Aldrich and was recrystallized twice from a solvent mixture of EtOH/H_2O (9:1) before being used in encapsulation experiments. The purity of pyrene was checked by time-resolved fluorescence experiments (λ_{ex} = 335 nm, λ_{em} = 383 and 395 nm) for a 0.5 μM pyrene solution in aerated water, where a monoexponential decay (133−135 ns) was observed. Poly(propylene glycol)bis(2-aminopropyl ether) (JEFFAMINE 2070) was received as a gift from Huntsman Inc. Cumene-terminated PSMA was purchased from Aldrich. Methanol (99.9%, spectro analyzed for use in UV range, Fisher Scientific) and ethanol (95%, Commercial Alcohols) were used as received, and aqueous solutions were prepared with deionized water (≥17.8 MΩ cm, Sybron Barnstead System).

4.1.2. Transmission Electron Microscopy. TEM images were obtained using a Tecnai Osiris scanning transmission electron microscope operating at 200 keV. For the nanoparticles dispersed in $CHCl_3$, a small amount of this dispersion was drop-cast on a carbon formvar-coated copper grid (400 mesh, Ted Pella, part # 01814-F) and air-dried before imaging. For samples dispersed in water, dilute colloids of the nanoparticles dispersed in water (5 μL) were placed on thin, carbon formvar-coated copper grids held by anticapillary tweezers (400 mesh, Ted Pella, part # 01814-F). Water was then slowly removed under reduced pressure overnight in a vacuum desiccator. For the uranyl acetate staining, the dried grid with an aqueous sample on it was held with anticapillary tweezers and a drop (5 μL) of saturated uranyl acetate aqueous solution was drop-casted onto the grid. A piece of absorbent tissue was placed underneath and in contact with the grid to adsorb extra uranyl acetate solution. Another drop (5 μL) of deionized water was placed on the grid, and again kimwipe was used to absorb the extra. The sample was then left in air for 5 min and used directly for imaging. The shape and size of the $NaYF_4$:ErYb nanoparticles and nanoassemblies were evaluated from the collected TEM images.

4.1.3. Dynamic Light Scattering. DLS measurements were carried out using Malvern Zetasizer Nano-ZS. The colloidal samples were held in a 10 mm path length plastic cuvette (BrandTech, Catalog # 759220). A nanoparticle concentration of ∼1 mg/mL was employed for the measurements.[a] DLS measurements were conducted at 25 °C.

4.1.4. Thermogravimetric Analysis. A typical TGA sample was prepared by removing an aliquot amount (1 mL) of the aqueous dispersion using a pipette to a clean scintillation vial and drying it under high vacuum at room temperature. When the sample was completely dry, the residue was dissolved in minimum amount of $CHCl_3$ and the solution was carefully transferred into the TGA heating pan, at which time the solution was completely evaporated in air before the TGA experiment was started. The TGA experiment was performed on a Shimadzu TGA-50 analyzer. The weight loss was analyzed by heating the sample from room temperature to 500 °C at the rate of 5 °C/min.

4.1.5. Optical Spectroscopy Sample Preparation. Concentrated pyrene stock solutions (∼1 mM) were prepared in methanol, and this stock solution was injected into deionized water to make solutions of 0.5 μM. The nanoassembly samples were used as prepared. All measurements were done in aerated solutions.

DOI: 10.1021/acsomega.8b00953
ACS Omega 2018, 3, 7673−7680

4.1.6. Synthesis of β-$NaYF_4$: 2 mol % Er^{3+}, 20 mol % Yb^{3+} Nanoparticles ($NaYF_4$:ErYb). In a typical synthesis, Y-$(CH_3CO_2)_3$ (3.9 mmol), $Yb(CH_3CO_2)_3$ (1.0 mmol), and $Er(CH_3CO_2)_3$ (0.1 mmol) were added to a 100 mL three-neck round-bottom flask containing 75 mL of octadecene and 30 mL of oleic acid. The solution was stirred magnetically and heated slowly to 120 °C under vacuum for 30 min to form the lanthanide oleate complexes and to remove residual water and oxygen. The temperature was then lowered to 50 °C, and the reaction flask was placed under a gentle flow of nitrogen gas. During this time, a solution of ammonium fluoride (0.74 g, 20 mmol) and sodium hydroxide (0.50 g, 12.5 mmol) dissolved in methanol (50 mL) was prepared via sonication. Once the reaction reached 50 °C, the methanol solution was added to the reaction flask and the resulting cloudy mixture was stirred for 30 min at 50 °C. The reaction temperature was then increased to 70 °C, and the methanol evaporated from the reaction mixture. Subsequently, the reaction temperature was increased to 300 °C as quickly as possible and maintained at this temperature for 60 min under the nitrogen gas flow. During this time, the reaction mixture became progressively clearer until a completely clear, slightly yellowish solution was obtained. The mixture was allowed to cool to room temperature. The nanoparticles were precipitated by the addition of ethanol and isolated via centrifugation at 4500 rpm corresponding to a relative centrifugal field (RCF) of approximately 1000. The resulting pellet was dispersed in a minimal amount of hexanes and precipitated with excess ethanol. The nanoparticles were isolated via centrifugation at 4500 rpm and then dispersed in chloroform for subsequent experiments.

*4.1.7. Synthesis of Hybrid Nanoassembly without Pyrene (**P1-NP**).* A stirring solution of cumene-terminated PSMA (25 mg, 0.016 mmol, M_n = 1700) in $CHCl_3$ (1 mL) was treated with JEFFAMINE 2070 (160 mg, 0.016 mmol, M_n = 2070) in $CHCl_3$ (1.0 mL), and the solution was stirred overnight at room temperature. The reaction mixture was then treated with a solution of the oleate-coated UCNPs ($NaYF_4$:ErYb) in $CHCl_3$ (250 μL, 42 mg/mL)[a] and stirred for 1 h. The reaction mixture was evaporated to dryness using a rotary evaporator. The oily residue was treated with aqueous NaOH (3 mL, 0.01 M, pH 12) and sonicated for 5 min, and any trace amounts of $CHCl_3$ were carefully removed using a rotary evaporator to afford a clear aqueous solution. This solution was transferred using a pipette into two 1.5 mL conical centrifugation tubes and centrifuged at 20 600 RCF for 25 min. The supernatant was removed from the pellets of nanoparticles using a pipette, and the pellets were redispersed in deionized water (3 mL for each sample) with the help of sonication. The tubes were centrifuged for 25 min at 20 600 RCF, and the supernatant was removed from the pellets of nanoparticles using a pipette. The nanoparticles were redispersed in deionized water (3 mL for each sample) with the help of sonication; the two samples were combined and passed through a 0.2 μm filter (Acrodisc syringe filter) to obtain the final stock solution of encapsulated nanoparticles for further characterization.

*4.1.8. Synthesis of Hybrid Nanoassembly with Pyrene (**P1-NP-pyr**, Two Batches).* A stirring solution of cumene-terminated PSMA (25 mg, 0.016 mmol, M_n = 1700) in $CHCl_3$ (1 mL) was treated with JEFFAMINE 2070 (160 mg, 0.016 mmol, M_n = 2070) in $CHCl_3$ (1.0 mL), and the solution was stirred overnight at room temperature. The reaction mixture was then treated with a solution of the oleate-coated UCNPs ($NaYF_4$:ErYb) in $CHCl_3$ (250 μL, 42 mg/mL)[2] and a stock solution of pyrene in $CHCl_3$ (1.4×10^{-3} M, 71 μL, 1×10^{-7} mol) and stirred for 1 h. The reaction mixture was evaporated to dryness using a rotary evaporator. The oily residue was treated with aqueous NaOH (3 mL, 0.01 M, pH 12) and sonicated for 5 min, and any trace amounts of $CHCl_3$ were carefully removed using a rotary evaporator to afford a clear aqueous solution. This solution was transferred using a pipette into two 1.5 mL conical centrifugation tubes and centrifuged at 20 600 RCF for 25 min. The supernatant was removed from the pellets of nanoparticles using a pipette, and the pellets were redispersed in deionized water (3 mL for each sample) with the help of sonication. The tubes were centrifuged for 25 min at 20 600 RCF, and the supernatant was removed from the pellets of nanoparticles using a pipette. The nanoparticles were redispersed in deionized water (3 mL for each sample) with the help of sonication; the two samples were combined and passed through a 0.2 μm filter (Acrodisc syringe filter) to obtain the final stock solution of encapsulated nanoparticles for further characterization.

4.1.9. Optical Spectroscopy. UV−vis spectra were recorded from 200−800 nm using Varian Cary 1 or Cary 100 spectrometers. Steady-state fluorescence emission spectra were collected using a PTI QM-40 fluorimeter. Emission spectra were recorded between 350 and 500 nm or 350−550 nm if excimer emission was observed, at excitation wavelengths of 331 or 335 nm. The step size was 0.25 nm, the integration time was 0.5 s, and the slits for both monochromators were set to either 1 or 2 nm bandwidths. The time-resolved emission decays were collected using an Edinburgh Instruments OB920 single photon counter. Samples were excited at 335 nm using an EPLED-330 light-emitting diode, and the emission decays were recorded at 400 nm. The emission monochromator slits were set to a bandwidth of 16 nm. The IRF was collected by recording the scattering of silica in a dilute LUDOX (Aldrich) solution and setting the emission wavelength to 335 nm to match the wavelength of the LED. Fluorescence experiments were carried out at 20 °C. The pyrene purity experiments were measured in 10 × 10 mm quartz cells, and 2 × 10 mm quartz cells were used for the UCNP experiments. For the latter, the cell faced the excitation beam so that the sample was irradiated through the 10 mm path length.

4.1.10. Data Fitting. The fluorescence decays were fit to a sum of exponentials (eq 1), and the quality of the fits was judged by the χ^2 values (0.9−1.2), and the randomness of the residuals.

$$I(t) = I_0 \sum_{1}^{i} A_i \, e^{-t/\tau_i} \tag{1}$$

Each fluorescent species has an associated lifetime (τ_i) and a pre-exponential factor (A_i), where the sum of the A_i values is unity. Reconvolution with the IRF was employed when analyzing the decay for the emission of the UCNP sample in the absence of pyrene, whereas a tail fit was used for the fit of the decay collected over longer time windows when pyrene was present because the excitation pulse is narrow for these experiments.

DOI: 10.1021/acsomega.8b00953
ACS Omega 2018, 3, 7673−7680

■ ASSOCIATED CONTENT

Supporting Information

The Supporting Information is available free of charge on the ACS Publications website at DOI: 10.1021/acsomega.8b00953.

Details on the instrumentation for analysis, and microscopy and spectral characterizations (PDF)

■ AUTHOR INFORMATION

Corresponding Authors

*E-mail: cornelia.bohne@gmail.com (C.B.).
*E-mail: nbranda@sfu.ca (N.R.B.).

ORCID

Cornelia Bohne: 0000-0001-9996-0076
Neil R. Branda: 0000-0003-2517-4165

Present Address

[‖]On sabbatical from Education Ministry Key Laboratory on Luminescence Real-Time Analysis, College of Chemistry and Chemical Engineering, Southwest University, Chongqing, China.

Author Contributions

[§]T.W. and J.O. contributed equally to this publication.

Notes

The authors declare no competing financial interest.

■ ACKNOWLEDGMENTS

This research was supported by the Natural Sciences and Engineering Research Council (NSERC) of Canada, the Canada Research Chairs Program, and Simon Fraser University. This work made use of 4D LABS shared facilities supported by the Canada Foundation for Innovation (CFI), British Columbia Knowledge Development Fund (BCKDF), and Simon Fraser University. Researchers at UVic thank NSERC (RGPIN-121389-2012) for funding and CAMTEC for the use of shared facilities.

■ ADDITIONAL NOTE

[a]This value was estimated based on assumption that all of the nanoparticles were transferred from the organic solution to the aqueous solution after the encapsulation process.

■ REFERENCES

(1) Petrosko, S. H.; Johnson, R.; White, H.; Mirkin, C. A. Nanoreactors: Small Spaces, Big Implications in Chemistry. *J. Am. Chem. Soc.* **2016**, *138*, 7443−7445.

(2) Roy, S.; Skoff, D.; Perroni, D. V.; Mondal, J.; Yethiraj, A.; Mahanthappa, M. K.; Zanni, M. T.; Skinner, J. L. Water Dynamics in Gyroid Phases of Self-Assembled Gemini Surfactants. *J. Am. Chem. Soc.* **2016**, *138*, 2472−2475.

(3) Williams, D. E.; Dolgopolova, E. A.; Pellechia, P. J.; Palukoshka, A.; Wilson, T. J.; Tan, R.; Maier, J. M.; Greytak, A. B.; Smith, M. D.; Krause, J. A.; Shustova, N. B. Mimic of the Green Fluorescent Protein *β*-Barrel: Photophysics and Dynamics of Confined Chromophores Defined by a Rigid Porous Scaffold. *J. Am. Chem. Soc.* **2015**, *137*, 2223−2226.

(4) Li, G.; Fu, C.; Oviedo, M. B.; Chen, M.; Tian, X.; Bekyarova, E.; Itkis, M. E.; Wong, B. M.; Guo, J.; Haddon, R. C. Giant Raman Response to the Encapsulation of Sulfur in Narrow Diameter Single-Walled Carbon Nanotubes. *J. Am. Chem. Soc.* **2016**, *138*, 40−43.

(5) Tagliazucchi, M.; Szleifer, I. How Does Confinement Change Ligand−Receptor Binding Equilibrium? Protein Binding in Nanopores and Nanochannels. *J. Am. Chem. Soc.* **2015**, *137*, 12539−12551.

(6) Ma, C.; Contento, N. M.; Bohn, P. W. Redox Cycling on Recessed Ring-Disk Nanoelectrode Arrays in the Absence of Supporting Electrolyte. *J. Am. Chem. Soc.* **2014**, *136*, 7225−7228.

(7) Wu, T.; Boyer, J.-C.; Barker, M.; Wilson, D.; Branda, N. R. A "plug-and-play" method to prepare water-soluble photoresponsive encapsulated upconverting nanoparticles containing hydrophobic molecular switches. *Chem. Mater.* **2013**, *25*, 2495−2502.

(8) Wu, T.; Barker, M.; Arafeh, K. M.; Boyer, J.-C.; Carling, C.-J.; Branda, N. R. A UV-Blocking Polymer Shell Prevents One-Photon Photoreactions while Allowing Multi-Photon Processes in Encapsulated Upconverting Nanoparticles. *Angew. Chem., Int. Ed.* **2013**, *52*, 11106−11109.

(9) Wu, T.; Wilson, D.; Branda, N. R. Fluorescent quenching of lanthanide-doped upconverting nanoparticles by photoresponsive polymer shells. *Chem. Mater.* **2014**, *26*, 4313−4320.

(10) Wu, T.; Johnsen, B.; Qin, Z.; Morimoto, M.; Baillie, D.; Irie, M.; Branda, N. R. Two-colour fluorescent imaging in organisms using self-assembled nano-systems of upconverting nanoparticles and molecular switches. *Nanoscale* **2015**, *7*, 11263−11266.

(11) Nyk, M.; Kumar, R.; Ohulchanskyy, T. Y.; Bergey, E. J.; Prasad, P. N. High Contrast in Vitro and in Vivo Photoluminescence Bioimaging Using Near Infrared to Near Infrared Up-Conversion in Tm3+ and Yb3+ Doped Fluoride Nanophosphors. *Nano Lett.* **2008**, *8*, 3834−3838.

(12) Haase, M.; Schäfer, H. Upconverting nanoparticles. *Angew. Chem., Int. Ed.* **2011**, *50*, 5808−5829.

(13) Demchenko, A. P.; Tang, K.-C.; Chou, P.-T. Excited-state proton coupled charge transfer modulated by molecular structure and media polarization. *Chem. Soc. Rev.* **2013**, *42*, 1379−1408.

(14) Kwon, J. E.; Park, S. Y. Advanced organic optoelectronic materials: harnessing excited-state intramolecular proton transfer (ESIPT) process. *Adv. Mater.* **2011**, *23*, 3615−3642.

(15) Hsieh, C.-C.; Jiang, C.-M.; Chou, P.-T. Recent Experimental Advances on Excited-State Intramolecular Proton Coupled Electron Transfer Reaction. *Acc. Chem. Res.* **2010**, *43*, 1364−1374.

(16) Rock, R. S.; Chan, S. I. Preparation of a Water-Soluble "Cage" Based on 3',5'-Dimethoxybenzoin. *J. Am. Chem. Soc.* **1998**, *120*, 10766−10767.

(17) Kalyanasundaram, K. *Photochemistry in Micro-heterogeneous Systems*; Academic Press: Orlando, 1987; p 388.

(18) Ramamurthy, V.; Inoue, Y. *Supramolecular Photochemistry: Controlling Photochemical Processes*; Wiley: Singapore, 2011; p 623.

(19) Pattabiraman, M.; Kaanumalle, L. S.; Ramamurthy, V. Photoproduct Selectivity in Reactions Involving Singlet and Triplet Excited States within Bile Salt Micelles. *Langmuir* **2006**, *22*, 2185−2192.

(20) Rinco, O.; Nolet, M. C.; Ovans, R.; Bohne, C. Probing the binding dynamics to sodium cholate aggregates using naphthalene derivatives as guests. *Photochem. Photobiol. Sci.* **2003**, *2*, 1140−1151.

(21) Amundson, L. L.; Li, R.; Bohne, C. Effect of the Guest Size and Shape on Its Binding Dynamics with Sodium Cholate Aggregates. *Langmuir* **2008**, *24*, 8491−8500.

(22) Kalyanasundaram, K.; Thomas, J. K. Environmental effects on vibronic band intensities in pyrene monomer fluorescence and their application in studies of micellar systems. *J. Am. Chem. Soc.* **1977**, *99*, 2039−2044.

(23) Dong, D. C.; Winnik, M. A. The Py Scale of Solvent Polarities. Solvent Effects on the Vibronic Fine Structure of Pyrene Fluorescence and Empirical Correlations with ET and Y Values. *Photochem. Photobiol.* **1982**, *35*, 17−21.

(24) Thomas, J. K. Effect of structure and charge on radiation-induced reactions in micellar systems. *Acc. Chem. Res.* **1977**, *10*, 133−138.

(25) Bohne, C.; Redmond, R. W.; Scaiano, J. C. *Photochemistry in Organized and Constrained Media*; VCH Publishers: New York, 1991; pp 79−132.

(26) See Supporting Information for details.

(27) The values for the average sizes were obtained directly from the DLS instrument using Malvern General Purpose & Multiple Narrow

DOI: 10.1021/acsomega.8b00953
ACS Omega 2018, 3, 7673−7680

Mode NNLS (non-negative least squares) algorithm to treat the autocorrelation equation of the intensity trace describing sample intensity fluctuation recorded during the experiment.

(28) These values are the total concentrations of pyrene encapsulated in the nanoassemblies obtained using the absorption of pyrene as measured by UV−vis absorption spectroscopy (λ = 335 nm) divided by the molar absorptivity of pyrene in acetonitrile (38 704 M^{-1} cm^{-1}), calculated from the data obtained in this study (see Supporting Information for details). The assumption is that the molar absorptivity of pyrene in acetonitrile is similar to that for pyrene in the nanoassembly.

(29) Mackay, D.; Shiu, W. Y. Aqueous solubility of polynuclear aromatic hydrocarbons. *J. Chem. Eng. Data* **1977**, *22*, 399−402.

(30) Winnik, F. M. Photophysics of preassociated pyrenes in aqueous polymer solutions and in other organized media. *Chem. Rev.* **1993**, *93*, 587−614.

(31) This shift is indicative of encapsulation of the chromophores within the amphiphilic polymeric structures as has been previously reported. See: Wilhelm, M.; Zhao, C. L.; Wang, Y.; Xu, R.; Winnik, M. A.; Mura, J. L.; Riess, G.; Croucher, M. D. Poly(styrene-ethylene oxide) block copolymer micelle formation in water: a fluorescence probe study. *Macromolecules* **1991**, *24*, 1033−1040.

(32) The I/III ratio depends on the resolution of the spectra, which is determined by the bandwidth of the emission monochromator. On the instrument used, a value close to 1.97 was obtained. For detailed discussion on experimental artifacts, see Street, K. W.; Acree, W. E. Experimental artifacts and determination of accurate Py values. *Analyst* **1986**, *111*, 1197−1201. For different reported I/III ratios, see refs 22 and 23

(33) Zou, W.; Visser, C.; Maduro, J. A.; Pshenichnikov, M. S.; Hummelen, J. C. Broadband dye-sensitized upconversion of near-infrared light. *Nat. Photonics* **2012**, *6*, 560−564.

(34) Yang, H.; Bohne, C. Effect of Amino-Acid Co-Inclusion on the Complexation of Pyrene with β-Cyclodextrin. *J. Phys. Chem.* **1996**, *100*, 14533−14539.

(35) Xu, W.; Demas, J. N.; DeGraff, B. A.; Whaley, M. Interactions of pyrene with cyclodextrins and polymeric cyclodextrins. *J. Phys. Chem.* **1993**, *97*, 6546−6554.

(36) Faulkner, S.; Carrié, M.-C.; Pope, S. J. A.; Squire, J.; Beeby, A.; Sammes, P. G. Pyrene-sensitised near-IR luminescence from ytterbium and neodymium complexes. *Dalton Trans.* **2004**, *9*, 1405−1409.

(37) Hueting, R.; Tropiano, M.; Faulkner, S. Exploring energy transfer between pyrene complexes and europium ions − potential routes to oxygen sensors. *RSC Adv.* **2014**, *4*, 44162−44165.

(38) Díaz, S. A.; Gillanders, F.; Jares-Erijman, E. A.; Jovin, T. M. Photoswitchable semiconductor nanocrystals with self-regulating photochromic Förster resonance energy transfer acceptors. *Nat. Commun.* **2015**, *6*, 6036.

DOI: 10.1021/acsomega.8b00953
ACS Omega 2018, 3, 7673−7680